

Supplementary Data

Food-waste-derived hydrochar to low-cost p-type semiconducting photocatalyst (Zn-Al@HC): Multifunctional role in real wastewater treatment and environmental sustainability

Shraddha Yadav^a, Monali Priyadarshini^a, Azhan Ahmad^b, Makarand M. Ghangrekar^{a, b*},
Brajesh Dubey^b

^a School of Environmental Science and Engineering, Indian Institute of Technology
Kharagpur, Kharagpur-721302, India.

^b Department of Civil Engineering, Indian Institute of Technology Kharagpur, Kharagpur-
721302, India.

* Corresponding author; E-mail address: ghangrekar@civil.iitkgp.ac.in

List of captions

Text S1. Synthesis of Zn-Al@HC photocatalyst

Text S2: Physicochemical, morphological, and electrochemical characterization

Text S3. UV/PDS/Zn-Al@HC photocatalytic degradation experiment and optimization

Text S4. Effect of aqueous matrix and residual sulfate (SO₄²⁻)

Fig. S1. N₂ adsorption-desorption isotherms and BJH pore size distributions of **(a – a1)** Zn-Al@HC and **(b – b1)** HC

Fig. S2. Optimization of SA photodegradation under **(a)** different systems, **(b)** PDS dose, **(c)** Zn-Al@HC dose, and **(d)** initial concentration of SA

Fig. S3. Kinetics of anions **(a)** chloride (Cl⁻), **(b)** fluoride (F⁻), **(c)** nitrate (NO₃⁻), **(d)** carbonate (CO₃²⁻), **(e)** phosphate (PO₄³⁻) in the photocatalytic degradation of SA in UV/PDS/Zn-Al@HC system

Fig. S4. Salicylic decay in the presence of **(a)** chloride, **(b)** fluoride, **(c)** nitrate, **(d)** carbonate, **(e)** phosphate

Fig. S5. **(a)** Photocatalytic performance of Zn-Al@HC in different water matrices, i.e., distilled water, tap water, and WWTP effluent, and **(b)** kinetics involved in the UV/PDS/Zn-Al@HC system

Fig. S6. LC-MS spectra of the **(a)** before photocatalytic degradation and **(b)** after photocatalytic degradation of the SA in the UV/PDS/Zn-Al@HC system

Table S1: Performance of HC-based photocatalyst in the photocatalytic degradation of emerging contaminants

Table S2: Theoretical chemical structure and m/z for the intermediates identified using LC-MS during the UV/PDS/Zn-Al@HC degradation of SA

Table S3: Operating cost and energy consumption for the SA degradation by different AOPs

Text S1: Synthesis of Zn-Al@HC photocatalyst

For preparation of Solution 1, ZnO (5.94 gm) was added to 10 mL of distilled water and Solution 2 was prepared by adding 15 gm of Al₂O₃ in 10 mL of distilled water. Solution 2 was then slowly mixed into Solution 1. Simultaneously, ammonia solution was added drop-wise and the solution was stirred using a magnetic stirrer until the attainment of pH of 9.0 for complete precipitation of the photocatalyst. Then, the as-synthesized photocatalyst was filtered, washed multiple times with distilled water, and oven-dried for 24 h at 105 °C to obtain the Zn-Al crystals. The above-synthesized photocatalyst was added to the AD-FW in the ratio of 1:30 (w/v) and both were immersed in 15 mL isopropyl alcohol. Further, the homogenization of the mixture was done using an ultrasonication bath at 50 °C for 45 min¹. After, ultrasonication the homogenized mixture was subjected to hydrothermal carbonization (HTC) in an autoclave at 210 °C for approximately 4 h. The composite HC obtained was then filtered, washed multiple times, and oven-dried at 105 °C for 12 h.

Text S2: Physicochemical, morphological, and electrochemical characterization

The crystalline phases through X-ray diffraction (XRD) patterns (X-ray diffractometer; Bruker D2 PHASER; Cu K_α radiation, $\lambda = 0.15418$ nm, scan angle range $2\theta = 10-90^\circ$, Germany). Surface functional groups and morphology of the catalysts were detected through Fourier transform infrared spectroscopy (FTIR; FTIR spectrometer; Nicolet 6700; Thermo Fisher Scientific, Germany) and Scanning electron microscopy (SEM; MERLIN, Zeiss, Oberkochen, Germany) operated at 10 kV and elemental constituents by Energy dispersive spectroscopy (EDS) operated at 15 kV, respectively². The surface elemental compositions and their respective chemical states in Zn-Al@HC were determined using the X-ray photoelectron spectroscopy (XPS) with a PHI-5000 VersaProbe III spectrophotometer (ULVAC-PHI INC, Kanagawa, Japan) using Al K_α X-ray source³.

The electrochemical analysis in terms of cyclic voltammetry (CV), Linear sweep voltammetry (LSV), chronoamperometry (CA), and Electrochemical impedance spectroscopy (EIS) were conducted in an electrochemical workstation (CHI 760D, CH Instruments, Inc., USA) using a 3-electrode system. The system comprised of glassy carbon electrode (GCE) modified with the prepared catalyst-working electrode; Ag/AgCl-reference electrode; and a Pt wire-counter electrode. The CV of the Zn-Al@HC was recorded at the potential window of -1 to 1 V, with scan rates of 10 mV s⁻¹, in O₂ saturated aqueous solution of 50 mM Na₂SO₄³.

Text S3. UV/PDS/Zn-Al@HC photocatalytic degradation experiment and optimization

The experiment was conducted in a dark cylindrical reactor having working volume of 1 L, placed on a magnetic stirrer at a rotation speed of 410 RPM. Initially, the Zn-Al@HC concentration was varied from 5 to 20 mg L⁻¹ with the constant initial dose of PDS (0.01 M). The photocatalytic degradation was conducted using 50 mg L⁻¹ initial concentration of model

pollutant (SA) and the solution was prepared using distilled water at neutral pH (~ 7.0) and room temperature (25 °C). The initial concentration of SA was adopted based on the previous work done by Priyadarshini et al. (2023).

The degradation pathway and probable intermediates of SA degradation by Zn-Al@HC catalyst were predicted using liquid chromatography-mass spectrometer (LC-MS, Thermo Fisher, LTQ-XL, India) and compared with the reported literature. The MS fragmentation data were collected in positive electrospray ionization mode and m/z range of 150 to 600⁵⁻⁷. To understand the role of reactive species $\cdot\text{OH}$ and $\text{SO}_4^{\cdot-}$, tert-butyl alcohol (TBA) as scavengers were adopted to eliminate the $\cdot\text{OH}$ radicals and methanol (MeOH) to scavenge both the $\text{SO}_4^{\cdot-}$ and $\cdot\text{OH}$ ⁸. The primary ROS generated in the system were investigated using Bruker pulsed Electron Paramagnetic Resonance (EPR) spectroscopy (ELEXSYS 580, USA). DMPO was employed as the spin-trapping reagent to capture $\text{SO}_4^{\cdot-}$ and $\cdot\text{OH}$. Further, the role of e^- , h^+ , and $\text{O}_2^{\cdot-}$ were evaluated using the quenching agents CCl_4 , $\text{Na}_2\text{-EDTA}$, and benzoquinone (BQ), respectively. The inhibition effect was evaluated for each scavenger.

Further, to evaluate the mineralization efficiency of SA, the Total organic carbon (TOC) was monitored with catalyst Zn-Al@HC concerning the irradiation time. The TOC content of the SA solution (experimented under the optimized condition), was analysed using the Shimadzu TOC-5000 analyser, USA⁹.

The optimization of SA initial concentration was performed for the 30, 50, 70, and 90 mg L⁻¹. Similarly, the effect of oxidant dosage was analysed for 0.005, 0.01, 0.015, and 0.02 M. Further the parameters were optimized and triplicate tests were performed for the accuracy of the results obtained. The effect of different operational parameters was analysed by varying one parameter at a time methodology. Control experiments were done to investigate the individual effect of Zn-Al@HC, UV, PDS, Zn-Al@HC/PDS, Zn-Al@HC/UV, UV/PDS, UV/Zn-Al@HC for further comparison with the present treatment.

Text S4. Effect of aqueous matrix and residual sulphate (SO_4^{2-})

The SA was spiked up to the concentration of 50 mg L⁻¹ in the three-water matrices, and the experiment was performed at the optimum condition of catalyst and oxidant dose for a reaction time of 150 min (including 30 min adsorption). Results showed (Fig. S4 (a, b)) the lower degradation efficiency of $78.19 \pm 0.10\%$ and $70.95 \pm 0.25\%$ in the wastewater treatment plant (WWTP) effluent and tap water matrix compared to the distilled water. These results suggest that the existence of conflicting reactions between the reactive radical species and the background species present in the selected water matrix decreased the available radicals for the effective degradation of SA. Moreover, the dissolved inorganics (halides, carbonates, bicarbonates) and organic matter can act as a site for absorbance/scattering of UV radiation. This can lead to a decrease in UV absorption by PDS for the generation of radicals or direct photolysis of the target compound SA. Additionally, the previous investigations reported the existence of organic matter played a crucial role in lowering the SA degradation efficiency than the inorganic matter. The lowest efficiency in the case of tap water can be ascribed to the

presence of alkalinity, which might negatively affect the SA degradation in the UV/PDS system.

The residual SO_4^{2-} concentration as determined in UV/PDS/Zn-Al@HC using ion chromatography (IC) was 554 mg L^{-1} , within the SO_4^{2-} discharge limits (typically range between 250 and 1000 mg L^{-1})¹⁰. However, for real field scalability SO_4^{2-} downstream treatment, such as ion exchange can be provided to decrease the residual sulphate concentration after the UV/PDS/Zn-Al@HC treatment¹¹.

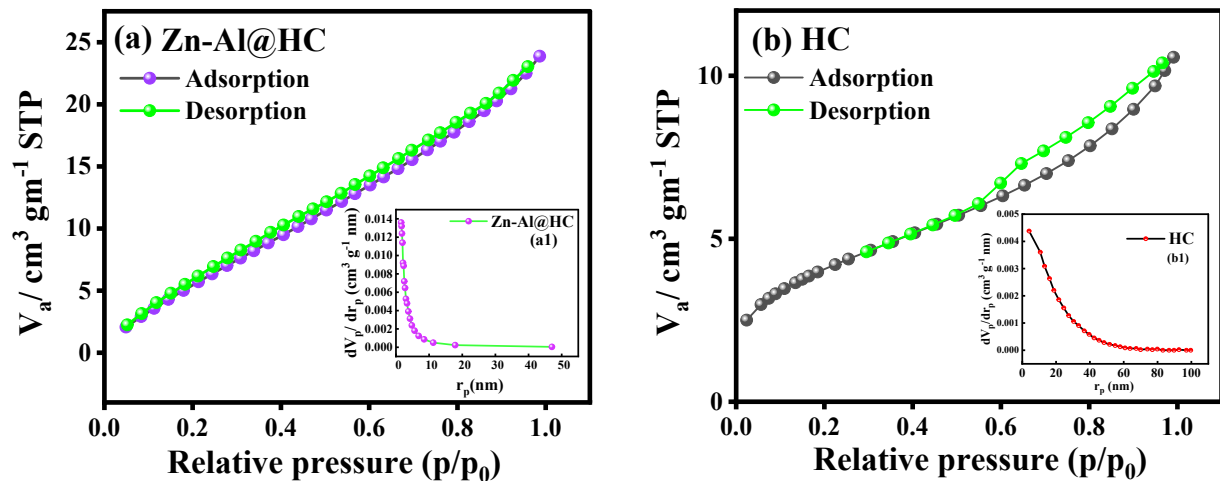


Fig. S1. N_2 adsorption-desorption isotherms and BJH pore size distributions of (a – a1) Zn-Al@HC and (b – b1) HC

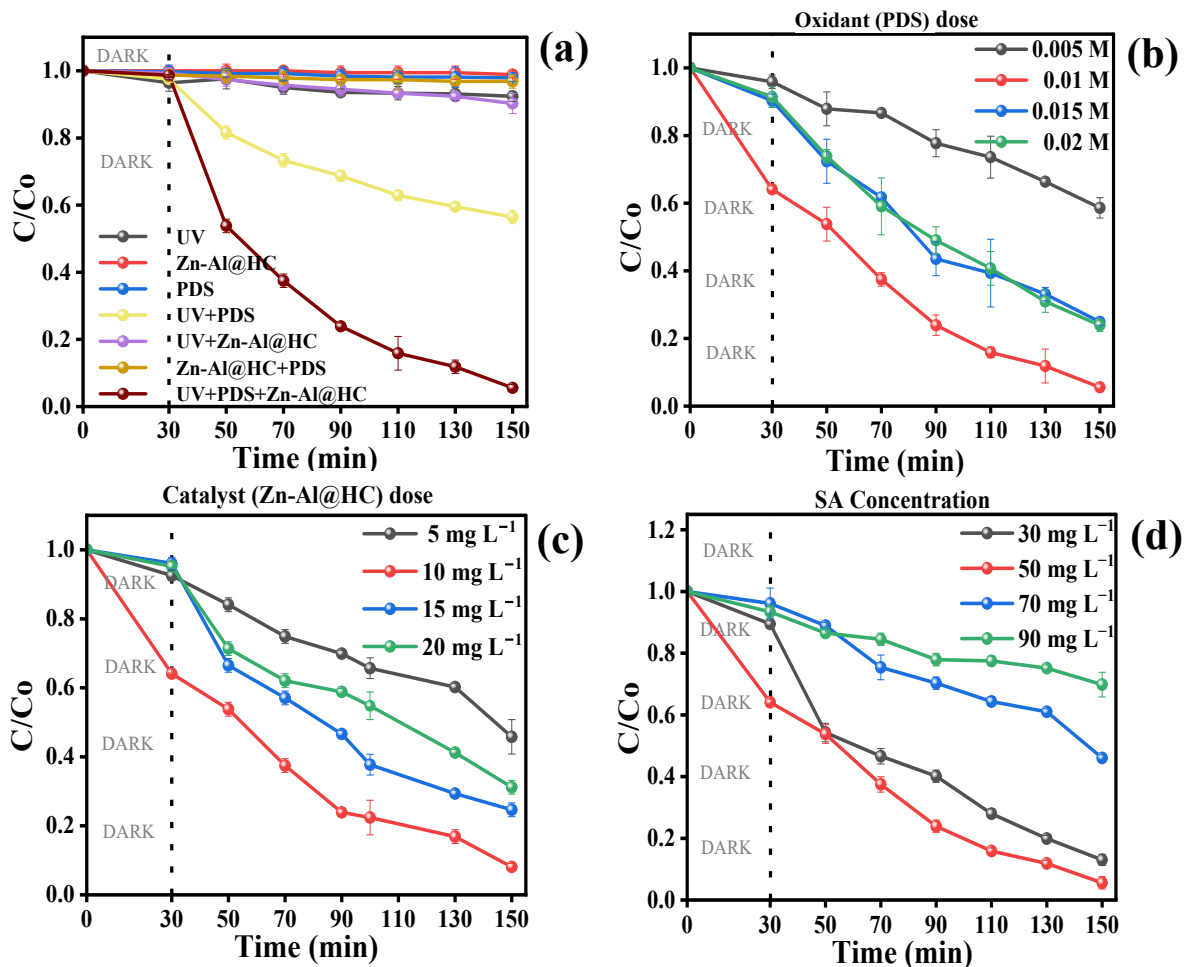


Fig. S2. Optimization of SA photodegradation under (a) different systems, (b) PDS dose, (c) Zn-Al@HC dose, and (d) initial concentration of SA.

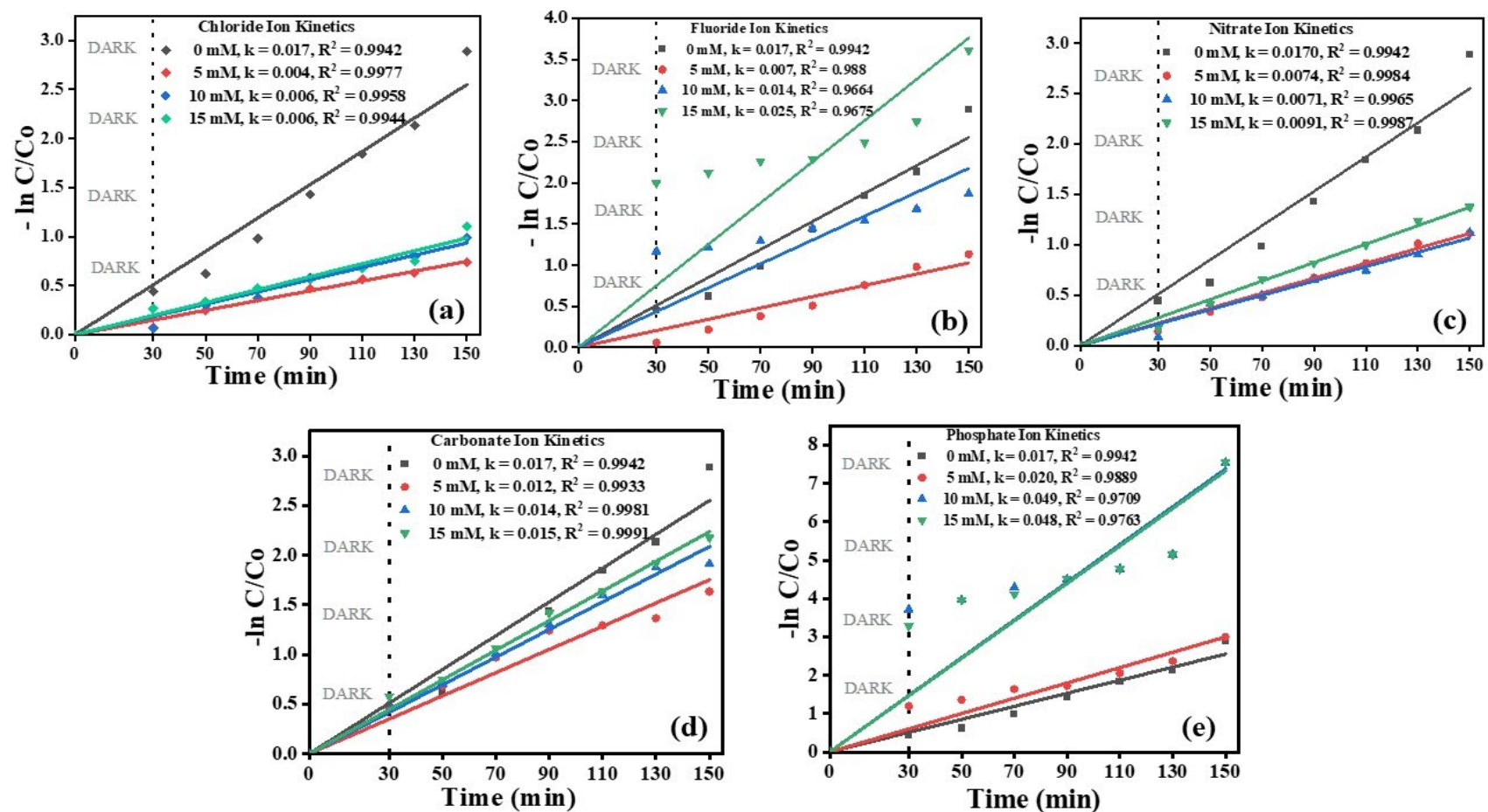


Fig. S3. Kinetics of anions (a) chloride (Cl^-), (b) fluoride (F^-), (c) nitrate (NO_3^-), (d) carbonate (CO_3^{2-}), (e) phosphate (PO_4^{3-}) in the photocatalytic degradation of SA in UV/PDS/Zn-Al@HC system. (Zn-Al@HC of 10 mg L^{-1} , UV fluence of $11 \mu\text{W cm}^{-2}$, PDS of 0.01 M , and SA of 50 mg L^{-1}).

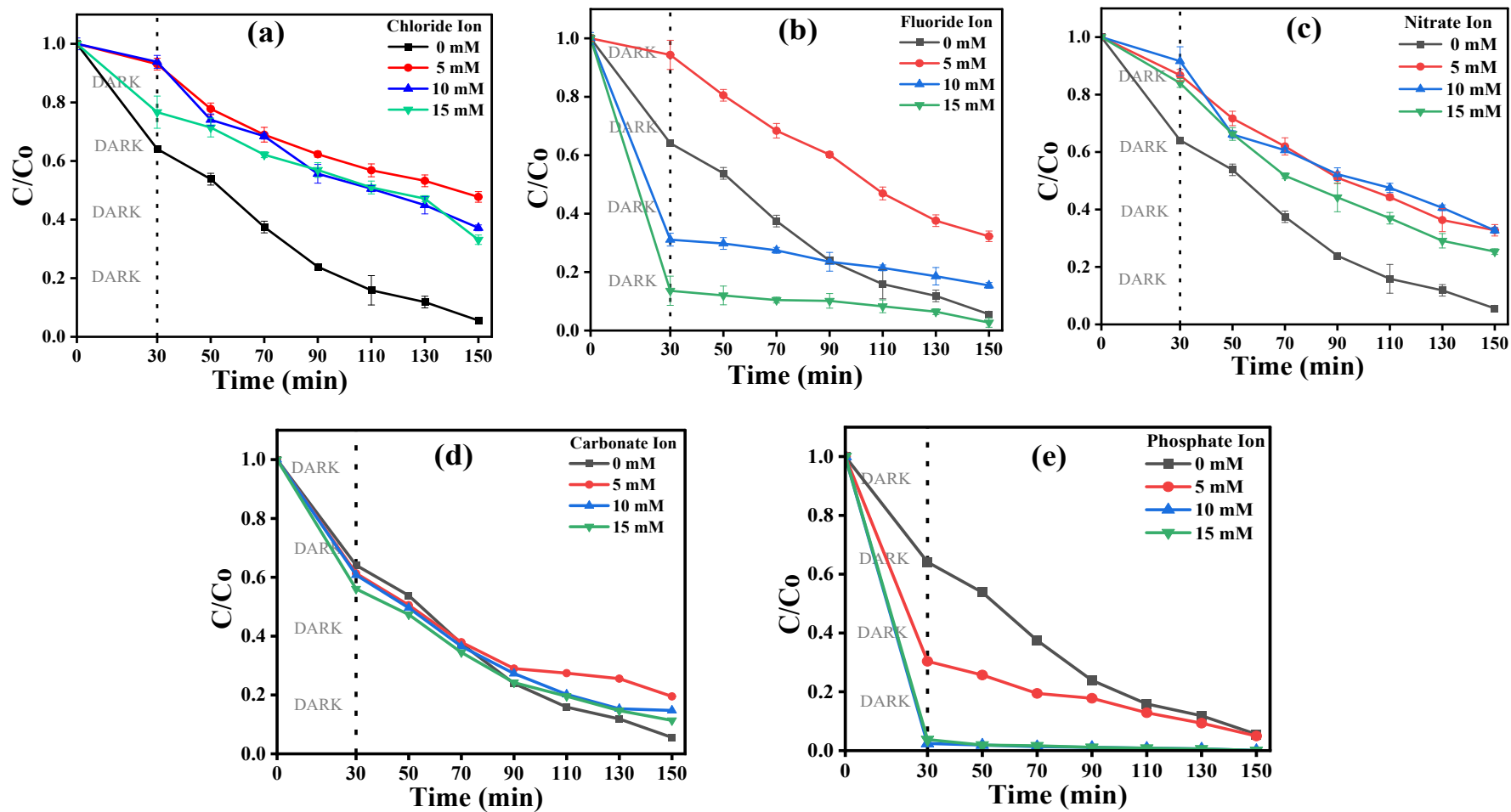


Fig. S4. Salicylic acid decay in the presence of (a) chloride, (b) fluoride, (c) nitrate, (d) carbonate, (e) phosphate (Zn-Al@HC of 10 mg L⁻¹, UV fluence of 11 μW cm⁻², PDS of 0.01 M, and SA of 50 mg L⁻¹).

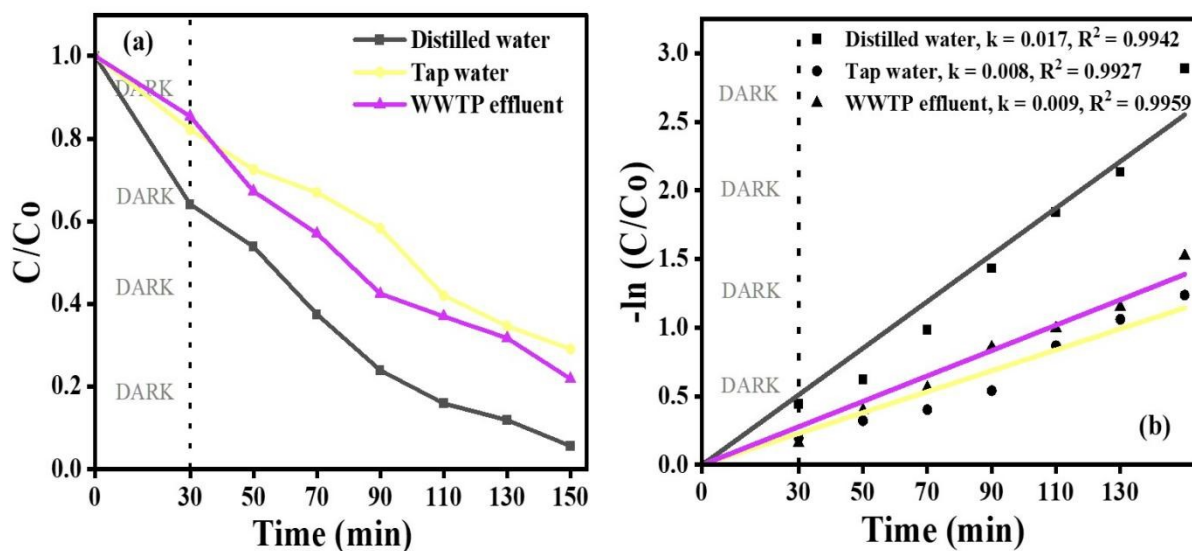


Fig. S5. (a) Photocatalytic performance of Zn-Al@HC in different water matrices, i.e., distilled water, tap water, and WWTP effluent, and (b) kinetics involved in the UV/PDS/Zn-Al@HC system (pH_0 of 7.0, temperature of 27 °C, Zn-Al@HC of 10 mg L⁻¹, UV fluence of 11 μ W cm⁻², PDS of 0.01 M, SA of 50 mg L⁻¹).

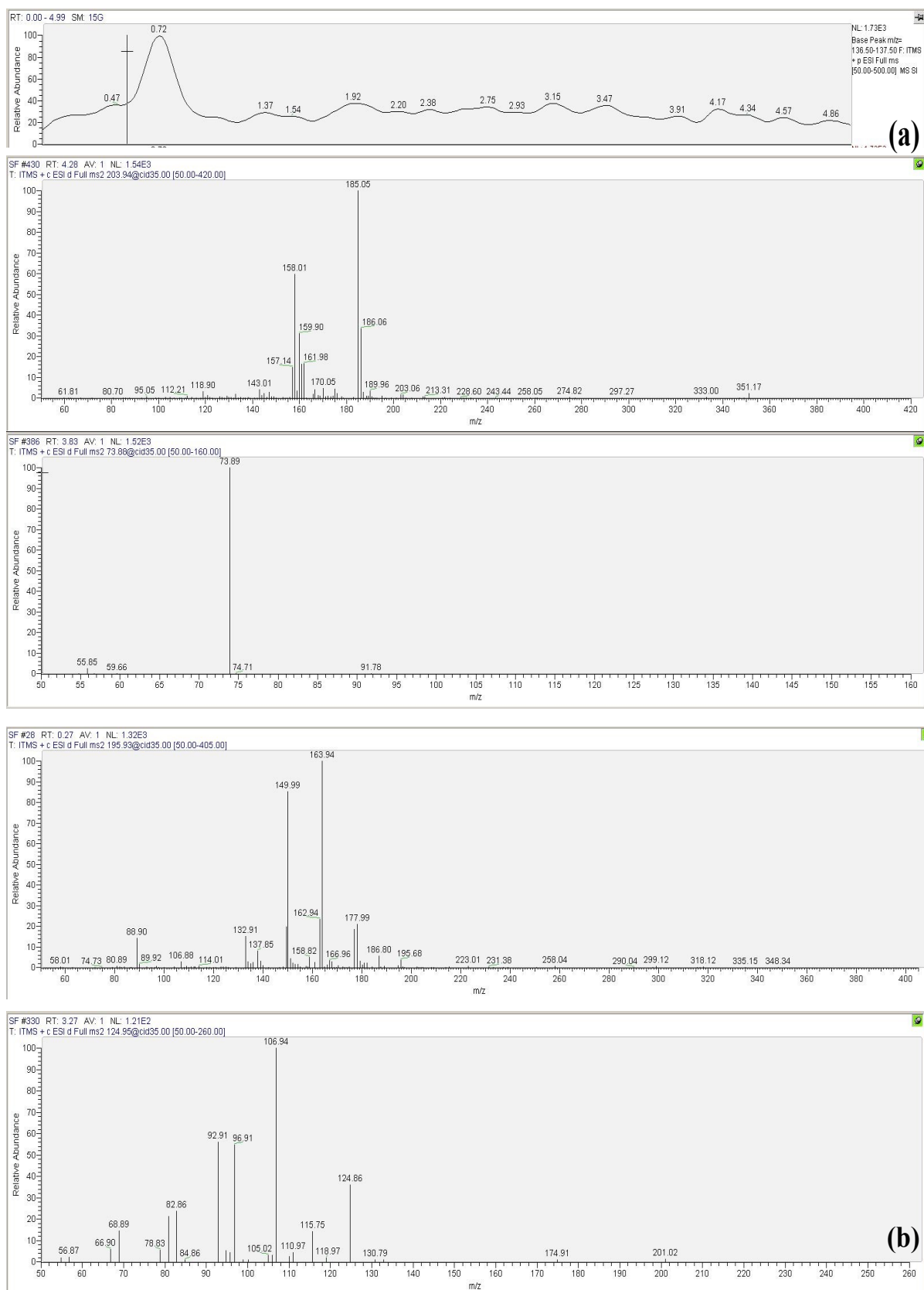


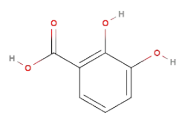
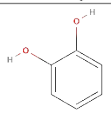
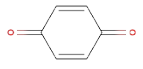
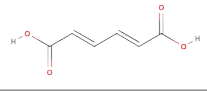
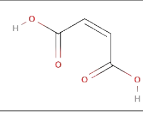
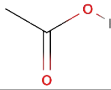
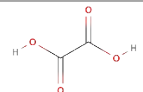
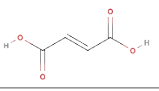
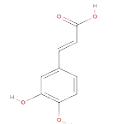
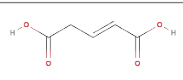
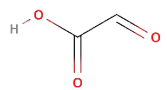
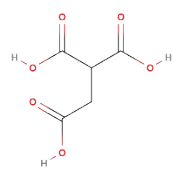
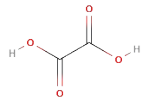
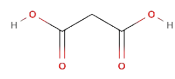
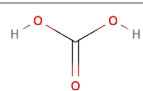
Fig. S6. LC-MS spectra of the **(a)** before photocatalytic degradation and **(b)** after photocatalytic degradation of the SA in the UV/PDS/Zn-Al@HC system

Table S1: Performance of HC-based photocatalyst in the photocatalytic degradation of emerging contaminants

HC-based Photocatalyst	Target contaminant	Experimental condition	Degradation efficiency (%)	References
Osmanthus fragrans HC/ Ag ₃ PO ₄	Sulfamethoxazole (SMX)	R _{time} = 90 min, R _{temperature} = 25 ± 2 °C, C _i = 1 mg L ⁻¹ , CD = 0.1 g L ⁻¹	98	12
Bamboo HC	Benzylamine	R _{time} = 32 h, R _{temperature} = 27 ± 2 °C, C _i = 1.9 mmol, CD = 20 mg	97.1	13
Fe ₃ O ₄ /BiOBr@HC	Carbamazepine	R _{time} = 40 min, R _{temperature} = 25 ± 2 °C, C _i = 10 mg L ⁻¹ , CD = 0.6 g L ⁻¹	100	14
Hazel nut HC/TiO ₂	Methylene blue	R _{time} = 420 min, R _{temperature} = 25 ± 2 °C, C _i = 10 mg L ⁻¹ , CD = 1 g L ⁻¹	96.97	15
Malt bagasse biomass HC/TiO ₂	Ramipril	R _{time} = 180 min, R _{temperature} = 25 °C, C _i = 50 mg L ⁻¹ , CD = 0.2 g L ⁻¹	96	16
Peanut shell HC /BiOBr/Bi ₁₂ TiO ₂₀	Rhodamine B	R _{time} = 160 min, R _{temperature} = 25 ± 2 °C, C _i = 10 mg L ⁻¹ , CD = 0.5 g L ⁻¹	98.55	17
Corn straw HC/FeAl LDH	Diethyl phthalate	R _{time} = 180 min, R _{temperature} = 27 °C, C _i = 20 mg L ⁻¹ , CD = 1 g L ⁻¹	68.9	18
Glucose-derived HC/KI	Perfluorooctanoic acid (PFOA)	R _{time} = 240 min, R _{temperature} = 25 °C, C _i = 12.4 mg L ⁻¹ , CD = 0.01 g L ⁻¹	99.5	19
Egg albumin HC/ FeWO ₄	Ciprofloxacin	R _{time} = 100 min, R _{temperature} = 25 °C, C _i = 20 mg L ⁻¹ , CD = 0.08 g L ⁻¹	92.23	20

Note: R_{time} = Reaction time, R_{temperature} = Reaction temperature, C_i = Initial concentration of contaminant, CD = Catalyst dose

Table S2: Theoretical chemical structure and m/z for the intermediates identified using LC-MS during the UV/PDS/Zn-Al@HC degradation of SA

Compound	Molecular mass (g mol ⁻¹)	Mass (m/z)	Chemical structure
2,3-dihydroxybenzoic	154	155,154	
Catechol	110	112	
1,4-benzoquinone	108	107	
Muconic acid	142	141, 143, 165	
Maleic acid	116	118, 139	
Acetic acid	60.52	60, 61	
Oxalic acid	90	113	
Fumaric acid	116	118	
Caffeic acid	180.16	135.18	
Glutaconic acid	130.10	131	
Oxoacetic acid	74.03	74	
Ethane-1,1,2-tricarboxylic acid	163.09	160	
Ethanedioic acid	90.03	90	
Propanedioic acid	104.06	105	
Carbonic acid	62.03	62	

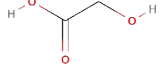
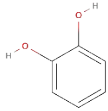
Hydroxyacetic acid	76.05	76	
2-hydroxy-1,4-benzoquinone	124.01	122, 124	

Table S3: Operating cost and energy consumption for the SA degradation by different AOPs

AOP	Time period (min)	SA conc. (mg L ⁻¹)	Degradation efficiency	EE ₀ (kWh m ⁻³)	References
Anodic oxidation with a BDD anode and a graphite cathode	360	164	100%	256	21
UV/Fenton	150	1000	98%	2.4 × 10 ⁴	22
UV/PDS and UV/Hydrogen peroxide	30	30	94% and 98%	77.1 and 57.83	23
Solar photoelectro-Fenton (SPEF) and solar heterogeneous photocatalysis (SPC)	360	165	87%	16.4	24
Electro-fenton	180	50		1.71	4
Peroxiocoagulation	100	50	69.5%	11.91	25
UV/PDS/Zn-Al@HC	150	50	94.45 ± 0.65%	0.74	Present investigation

References

- 1 S. Siara, C. Elvis, R. Harishkumar and P. Velayudhaperumal Chellam, *Mater. Res. Bull.*, 2022, **145**, 111530.
- 2 S. Mergenbayeva, A. Zakharova, A. Tynysbek, L. H. Koole, T. S. Atabaev and S. G. Poulopoulos, *Mater. Today Proc.*, **71**, 119-123.
- 3 I. Chakraborty, D. Ghosh, S. M. Sathe, B. K. Dubey, D. Pradhan and M. M. Ghangrekar, *Electrochim. Acta*, 2021, **398**, 139341.
- 4 M. Priyadarshini, A. Ahmad and M. M. Ghangrekar, *Environ. Pollut.*, 2023, **322**, 121242.
- 5 M. Petrovic, M. Petrovic and D. Barceló, *TrAC - Trends Anal. Chem.*, 2007, **26**, 486–493.
- 6 P. Bansal, D. Singh and D. Sud, *Sep. Purif. Technol.*, 2010, **72**, 357–365.
- 7 W. Wang, Q. Zhu, F. Qin, Q. Dai and X. Wang, *Chem. Eng. J.*, 2018, **333**, 226–239.
- 8 S. Verma and R. K. Dutta, *J. Environ. Chem. Eng.*, 2017, **5**, 4776–4787.
- 9 N. O. Diaz, C. A. Rodríguez, J. C. Durán-Álvarez, N. Talreja, I. Quispe-Fuentes, C. Martínez-Avelar, M. Bizarro, H. Valdés and A. C. Mera, *Mater. Sci. Eng. B Solid-State Mater. Adv. Technol.*, 273, 115432.
- 10 E. T. Nurmesniemi, M. Huhta, M. Derkani, V. Isteri, T. Hanein, T. Hu, P. Tanskanen and U. Lassi, *Front. Mater.*, 2022, **9**, 1–11.
- 11 A. R. Ishak, S. W. Khor, S. Mohamad and K. S. Tay, *Environ. Technol. Innov.*, 2021, **24**, 102065.
- 12 L. Zhou, M. Cai, X. Zhang, N. Cui, G. Chen and G. Y. Zou, *RSC Adv.*, 2019, **9**, 35636–35645.
- 13 F. Su, H. Peng, H. Yin, C. Luo, L. Zhu, W. Zhong, L. Mao and D. Yin, *J. Catal.*, 2021, **404**, 149–162.
- 14 S. Li, Q. Ma, L. Chen, Z. Yang, M. Aqeel Kamran and B. Chen, *Chem. Eng. J.*, 2022, **433**, 134492.
- 15 Y. O. Donar, S. Bilge, A. Sinağ and O. Pliekhov, *ChemCatChem*, 2018, **10**, 1134–1139.
- 16 J. Leichtweis, S. Silvestri, N. Stefanello and E. Carissimi, *Chemosphere*, 2021, **281**, 130987.
- 17 Y. Ren, X. Liu, H. Li, X. Wang and X. Jing, *Chem. Phys. Lett.*, 2022, **797**, 139584.
- 18 Q. Ye, Z. Huang, P. Wu, J. Wu, J. Ma, C. Liu, S. Yang, S. Rehman, Z. Ahmed, N. Zhu and Z. Dang, *J. Hazard. Mater.*, 2020, **388**, 122120.
- 19 Y. Hu, Y. Zhan, C. Wei, F. Chen, J. Cheng, Y. Shen, Z. Zhou, L. Wang and Y. Liang, *Sci. Total Environ.*, 2023, **868**, 161621.
- 20 T. Ahamad, M. Naushad and S. M. Alshehri, *Chem. Eng. J.*, 2021, **417**, 127969.
- 21 E. Guinea, C. Arias, P. L. Cabot, J. A. Garrido, R. M. Rodríguez, F. Centellas and E. Brillas, *Water Res.*, 2008, **42**, 499–511.
- 22 C. L. P. S. Zanta and C. A. Martínez-Huitle, *Brazilian J. Chem. Eng.*, 2009, **26**, 503–513.
- 23 J. Saien, M. Osali and A. R. Soleymani, *Desalin. Water Treat.*, 2015, **56**, 3087–3095.

- 24 B. Garza-Campos, E. Brillas, A. Hernández-Ramírez, A. El-Ghenymy, J. L. Guzmán-Mar and E. J. Ruiz-Ruiz, *J. Hazard. Mater.*, 2016, **319**, 34–42.
- 25 İ. Y. Köktaş and Ö. Gökkuş, *Chemosphere*, 2022, **293**, 133566.